ChemComm

Exfoliation, Delamination, and Oxidation Stability of Molten Salt Etched Nb2CTz MXene Nanosheets

Journal:	*ChemComm*
Manuscript ID	CC-COM-04-2022-002237.R2
Article Type:	Communication

SCHOLARONE™
Manuscripts

Please do not adjust margins

COMMUNICATION

Exfoliation, Delamination, and Oxidation Stability of Molten Salt Etched Nb_2CT_z MXene Nanosheets

Kailash Arole[1], Jackson W. Blivin[2], Atiana M. Bruce[2], Swarnima Athavale[2], Ian J. Echols[2], Huaixuan Cao[2], Zeyi Tan[1], Miladin Radovic[1], Jodie L. Lutkenhaus[1,2], Micah J. Green[*1,2]

Received 00th January 20xx,
Accepted 00th January 20xx

DOI: 10.1039/x0xx00000x

Despite numerous prior reports of molten salt etching of MAX phases, few of these reports achieved water-dispersible MXene nanosheets, and none for Nb-based MXenes. Here we demonstrate the synthesis and aqueous dispersibility of Nb_2CT_z nanosheets via molten salt etching and utilizing a KOH wash to add hydroxyl surface groups. However, little is known about the oxidation of molten salt etched MXenes compared to acid-etched MXenes. Our results indicate slower oxidation behavior for MXenes etched by molten salts, which may be due to the decreased amount of oxygen-containing terminal groups.

The safe and scalable production of MXenes has been an important but elusive goal since the first MXene synthesis in 2011[1]. MXenes are 2D nanomaterials with the general formula of $M_{n+1}X_nT_z$, where M is an early transition metal (typically Ti, Nb, or V), X is carbon and/or nitrogen, and T_z represents surface terminations (*e.g.,* -F, -Cl, -OH, -O). MXenes are derived from a parent material called the MAX phase, which combines the M-X with an interlayer (A) element from periodic groups 13-16 [2,3]. Over 50 MAX phases have been synthesized; however, only some MAX phases can be exfoliated into the 2D MXene nanosheets of interest with traditional acid etching techniques. Most prior research has focused on Ti-based MXenes. MXene nanosheets can be used for a range of applications such as energy storage, catalysis, EMI shielding, sensors, and composites [4-10].

High concentration hydrofluoric acid (HF) is commonly used to selectively remove the A layer from the MAX phase to produce MXenes. Other methods often use salts to form an *in situ* HF solution, such as combining lithium fluoride (LiF) and hydrochloric acid (HCl) or using ammonium bifluoride $(NH_4)HF_2$ [1,11]. However, the use of aqueous fluoride-based etchants has many inherent risks and challenges. The hazards related to the handling of HF make the MXene synthesis process difficult to scale up to a commercial level. Another disadvantage of the acid-etched MXene synthesis route is waste management [12]. In addition, the traditional HF acid etching technique is restricted to only a few MAX phases, so there is a need to explore alternative etching methods such as electrochemical exfoliation, hydrothermal etching, and molten salt etching [13-16].

The first use of molten salts to etch the MAX phase was in 2016 by Urbankowski *et al.* Using a mixture of fluoride salts, they created the first Ti_4N_3 nitride MXenes [17]. In 2019, Li *et al.* synthesized $Ti_3C_2T_z$ MXene with $ZnCl_2$, a salt that acts as a Lewis acid when in a molten state [18]. However, they were unable to delaminate the MXene clay (non-delaminated MXene) into single or multi-layer nanosheets and were unable to etch other MAX phases (Ti_2AlC, Ti_2AlN, V_2AlC) [18]. Soon after, Li *et al.* expanded on this work by computing the capabilities of Lewis acid molten salts for etching MAX phase [19]. After calculating which chloride salts would successfully etch a range of MAX phases, they etched several Ti-based MAX (Ti_2AlC, Ti_3ZnC_2, Ti_3AlC_2, Ti_3AlCN, Ta_2AlC) phases using the salts: $CuCl_2$, $NiCl_2$, $FeCl_2$, and AgCl. However, none of the MXene clays created were delaminated into nanosheets [19]. Kamysbayev *et al.* also used molten salts with different halogens to tailor the terminal groups of MXenes[20]. This study delaminated the etched MXene clay and dispersed the nanosheets in N-methylformamide (NMF) [20]. This was the first study to report both delamination and dispersion of molten-salt-derived MXenes in a liquid, with both single- and few-layer nanosheets present. The MAX phases that were etched into MXenes included Ti_3AlC_2, Ti_2AlC, and Nb_2AlC. However, aqueous dispersions were not demonstrated. The waster dispersibility of MXene is important for various applications such as water-based inks and spray coating[21].

In 2021, our group etched Ti_3AlC_2 with SnF_2 as the molten salt. Then, utilizing a KOH wash to attach -OH groups to the surface of the $Ti_3C_2T_z$, we were able to create a stable aqueous dispersion [16]. This was the first-time salt etched MXenes were able to be dispersed in water. We were also able to achieve extraordinary interlayer spacing in Nb_2CT_z clay due to the intercalation of Sn between layers.

However, no one has been able to demonstrate HF-free synthesis of water-dispersible Nb-based MXenes to date. Here, we demonstrate the versatility of our technique by producing Nb_2CT_z via molten salt (SnF_2) etching, yielding not only Nb_2CT_z clay but also delaminated water-dispersible nanosheets. To achieve this, we utilize a KOH wash to add -OH groups on the Nb_2CT_z surface. Instead of using traditional intercalants such as Dimethyl Sulfoxides (DMSO) and Tetrabutylammonium hydroxide (TBAOH), an aqueous solution of isopropylamine (i-PrA) was used. This salt etching method has an enhanced yield of 10-15% at 36 hr, in contrast to the traditional aqueous HF etching method with yields of ~10% at 70 hr [22].

[1]*Department of Materials Science and Engineering, Texas A&M University, College Station, TX 77843, USA;*
[2]*Artie McFerrin Department of Chemical Engineering, Texas A&M University, College Station, TX 77843, USA*
**Corresponding author: micah.green@tamu.edu*
Electronic Supplementary Information (ESI) available: [details of any supplementary information available should be included here]. See DOI: 10.1039/x0xx00000x

Please do not adjust margins

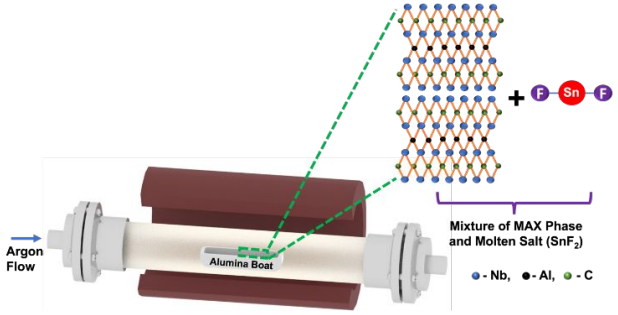

Figure 1. Schematic of tube furnace used for molten salt etching of Nb_2CT_z.

The molten salt etching of Nb_2CT_z was carried out as follows: a mixture of Nb_2AlC and SnF_2 (1:6 molar ratio) was heated in an argon atmosphere inside the tube furnace at a temperature of 750 °C for 36 hr. **(Figure 1).** The etched Nb_2CT_z clay was dispersed into a 0.1M potassium hydroxide (KOH) solution and stirred for about 2 hr to add -OH terminal groups and remove unreacted SnF_2 salt. After KOH treatment, the Nb_2CT_z clay was washed with water and then dispersed in an aqueous solution of i-PrA for intercalation. After intercalation, the Nb_2CT_z clay was washed with water to remove residual i-PrA, delaminated by bath sonication, and centrifuged at 3,500 rpm for 1 hr. After centrifugation, the supernatant (Nb_2CT_z nanosheets) was collected and freeze-dried to obtain a powder.

The earlier work by Li *et al.* has proposed the mechanism for the formation of halide terminated $Ti_3C_2T_z$ MXene via a molten salt etching approach and we have proposed a similar mechanism in our earlier work on fluorine terminated $Ti_3C_2T_z$[16,18]. The formation of F-terminated Nb_2CT_z via molten salt etching is also a two-step reaction. First, **step 1** involves the replacement of Al in Nb_2AlC by Sn, which results in the formation of Nb_2SnC, an intermediate product of Nb_2CT_z, along with AlF_3 as a by-product is generated. Also, as the reaction proceeds, Sn^{2+} ions form, which will intercalate into the A site after removing Al from Nb_2AlC. In **step 2**, the intermediate phase, Nb_2SnC gains F-terminations in the presence of an excess of SnF_2 salt.

Step 1: $Nb_2AlC + 1.5SnF_2 \rightarrow Nb_2SnC + AlF_{3\,(g)} + 0.5Sn$

Step 2: $Nb_2SnC + SnF_2 \rightarrow Nb_2CF_2 + 2Sn$

The morphology of the Nb_2AlC MAX phase and etched Nb_2CT_z is shown in **Figure 2**. The scanning electron microscope (SEM) image of the parent Nb_2AlC MAX phase, used to synthesize Nb_2CT_z, has a compact layered structure (**Figure 2a**). To determine the kinetics of the etching of Nb_2CT_z, we varied the etching time from 6 hr to 36 hr while keeping the etching temperature constant at 750 °C. All etching times at 750 °C resulted in the formation of the classic accordion-like structure (**Figure 2b**, **Figure 2c, Figure S1**). The accordion-like structure and expansion along the basal planes indicate the successful removal of the Al layer and the formation of Nb_2CT_z. In the case of Nb_2CT_z etched for 6 hr, 12 hr, and 24 hr, we observed impurities such as AlF_3, unreacted SnF_2, and Sn spheres (**Figure S1**). We observed less expansion along the basal planes (from SEM) in those Nb_2CT_z clays compared to Nb_2CT_z etched for 36 hr.

The decrease in the wt. % of Al indicates the successful removal of the A layer from the parent Nb_2AlC to form Nb_2CT_z (**Tables S1-S3, Table 1**). The presence of a minute amount of Al in the Nb_2CT_z can be attributed to residual unetched MAX phase and AlF_3.

MXene colloidal stability is essential for a range of applications, including printing ink or sprayed coatings[23]. In the case of molten salt etched MXenes, we hypothesize that the lack of -OH groups on the Nb_2CT_z is the reason that a stable aqueous dispersion of nanosheets is difficult to obtain. In order to add hydroxyl groups and allow for a stronger ζ-potential, we introduced a KOH washing step. The KOH washing not only adds -OH groups to the Nb_2CT_z clay but also aids in the removal of unreacted molten salt from the product [16].

We then explored the exfoliation of Nb_2CT_z clay by intercalation of i-PrA to reduce the interaction between the layers after etching. The i-PrA was selected because it forms the ammonium cation R-NH_3^+ when mixed with water, which can intercalate between the Nb_2CT_z layers. Also, the smaller size of the i-PrA cation allows for easier intercalation, pushing the MXene layers apart to ease the delamination process and result in the formation of Nb_2CT_z nanosheets. After treating the Nb_2CT_z with KOH and intercalating with i-PrA, we obtained a stable Nb_2CT_z nanosheet dispersion with a zeta (ζ) potential of (–41.3 ± 3.3) mV (**Figure 3a**) and hydrodynamic diameter of (270 ± 27) nm (**Figure 3b**). The negative zeta potential stems largely from the -OH terminal groups.

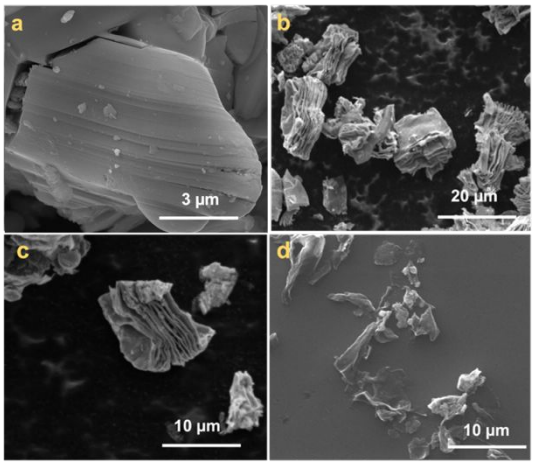

Figure 2. Scanning Electron Microscopy images of Nb_2AlC MAX phase and Nb_2CT_z etched for 36 hours. (a) Nb_2AlC MAX phase; (b) Nb_2CT_z clay before KOH washing and (c) Nb_2CT_z clay after KOH washing; (d) Nb_2CT_z nanosheets.

Table 1. The elemental composition of Nb_2CT_z (36 hr etched) before and after KOH wash and after separation was obtained by EDS.

Nb_2CT_z	Before KOH wash	After KOH wash	Nb_2CT_z Nanosheets
Element	**% Weight**	**% Weight**	**% Weight**
Nb	34.2	42.5	47.5
Sn	6	5.8	1.9
F	4.7	12.9	11
O	18.2	13.9	15.5
C	32.6	22.2	22.9
Al	4.4	2.8	1.5

The colloidal dispersion of Nb_2CT_z nanosheets was diluted and drop-cast on silicon wafers for SEM imaging. We found the presence of small particles (**Figure S1**) around the Nb_2CT_z nanosheets etched for 6, 12, and 24 hr. Interestingly, the 36 hr etched Nb_2CT_z nanosheets dispersion did not show any large amount of impurities in the SEM (**Figure 2d).** We hypothesize that the complete etching of the MAX phase resulted in a purer MXene, with no unreacted salt or impurities. The additional SEM images of Nb_2CT_z nanosheets are shown in **Figure S2.** The Nb_2CT_z etched for 36 hr had an elemental composition of (**Table 1**) Nb:C:F = 47.2:22.9:11 (wt.%). The only unusual feature is the presence of Sn and Al when compared with acid-etched Nb_2CT_z MXenes. Multiple water washes can reduce the % of Sn and Al impurities in the final product. Based on the amount

This journal is © The Royal Society of Chemistry 20xx

of Al removed (measured by EDS), the Nb_2CT_z clay yield was around 76%, and based on Nb_2CT_z nanosheet mass in the final product; the yield was 10% – 15%. The Raman data (**Figure S3**) shows the characteristic peaks of Nb_2CT_z at 452 cm^{-1} and 641 cm^{-1} [24-27]. An additional peak of Nb_2O_5 was also observed at 947 cm^{-1}, and this small oxide peak is attributed to the high-temperature etching [28]. The two broad peaks at 1356 cm^{-1} and 1589 cm^{-1} were observed and could be assigned to characteristic peaks of D and G bands of carbon species. The intensity ratios of the D band to the G band (I_D/I_G) of the Nb_2CT_z were found to be 1.23.

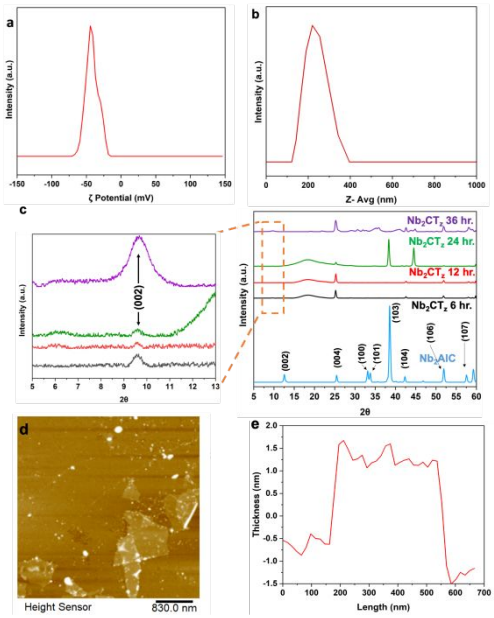

Figure 3. (a) ζ potential; (b) DLS of Nb_2CT_z nanosheet dispersion of 36 hr; (c) XRD of Nb_2AlC MAX phase and Nb_2CT_z nanosheets at different etching times; (d) atomic force microscopy (AFM) of Nb_2CT_z nanosheets dispersion; (e) corresponding height profile. Nb_2CT_z dispersion (0.006 mg/ml) was diluted with water and drop-cast on a silica wafer.

Figure 3c shows the X-ray diffraction pattern of the Nb_2AlC MAX phase, which is used for etching, and various basal plane peaks associated with the structure of the parent MAX phase are listed in the graph. The etching of Nb_2CT_z was studied by X-ray diffraction (XRD) (**Figure 3c**). The (002) peak associated with the Nb_2AlC MAX phase shifted from 2θ = 12.5° to 9.5°, confirming the formation of Nb_2CT_z. Also, the intensity of the MAX phase peak at 39° is reduced in the case of etched Nb_2CT_z, indicating the removal of Al in the as-prepared nanosheets. The presence of the (004) peak is attributed to the formation of some Nb_2O_5, which might have formed due to high etching temperature. The presence of MAX phase peak in case of 24 hours etched Nb_2CT_z MXene batch is very unusual. The presence of some non-basal peaks is attributed to the presence of a few multilayers. We observed no intense peaks for Sn after etching, intercalation, and delamination steps; this shows the successful removal of Sn impurities from the final Nb_2CT_z.

The thickness of the Nb_2CT_z nanosheets was studied by AFM (**Figures 3d, e**). The AFM data indicated that the thickness of obtained nanosheets is 1.5 nm, which agrees with the literature[29]. A few bright spots were observed in AFM images which are attributed to the crumbling of the edges of the nanosheets during the drying process. Another possibility is that the shiny sphere-like morphology in the AFM images is due to Sn impurities in the Nb_2CT_z dispersion.

Previously our group showed that the change in absorbance of dispersion could be used to study the kinetics of the oxidation [22]. The change in the absorbance value over a period was used to study the oxidation of the dispersion. An oxidation study of molten salt etched Nb_2CT_z nanosheets was carried out by examining the change in the absorbance of the dispersion over time (**Figures 4a**, **S4**). Absorbance was measured regularly at 776 nm to determine the extent of oxidation and measurements of absorbance were carried out multiple times before data fitting. There was a 23% decrease in absorbance over a storage time of 200 hr. This is relatively small compared to the drop in absorbance for acid-etched Nb_2CT_z nanosheets, which was around 58% over a period of 200 hr [22]. This difference in the absorbance trend between acid-etched and molten salt etched Nb_2CT_z nanosheets can be attributed to the difference in their surface terminal groups; acid-etched Nb_2CT_z are usually terminated with -O-, -OH, -F groups, whereas molten salt etched Nb_2CT_z are usually terminated with -F, -Cl, -Br, and -OH groups. Oxygen-containing terminal groups like -O- and -OH are responsible for the rapid oxidation of MXene.[30] The Tyndall scattering effect (**Figure 4b**) was observed, confirming the colloidal dispersion of Nb_2CT_z nanosheets.

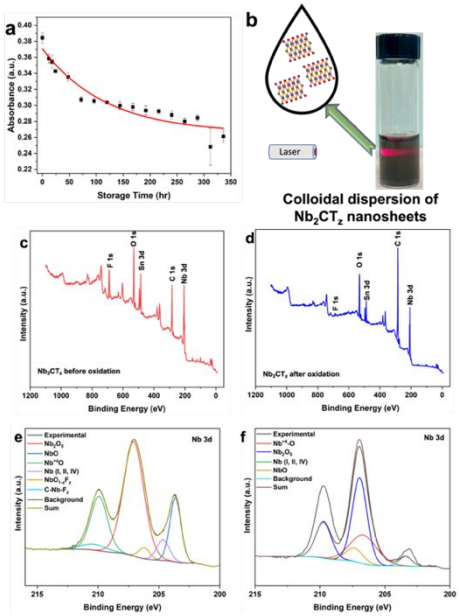

Figure 4. (a) The UV – vis absorbance of Nb_2CT_z dispersion at different storage times. Points represent experimental data and lines represent a model fit using $A = A_0 + A_1 \exp(-t/\tau)$; (b) Tyndall scattering; Survey spectra of the (c) As-prepared (d) 300 hr aged Nb_2CT_z; Deconvoluted Nb 3d spectra of (e) As-prepared; (f) 300 hr aged Nb_2CT_z nanosheets dispersion.

The oxidation behavior of molten salt etched Nb_2CT_z was examined by XPS, measuring the oxide content of the Nb_2CT_z (**Figure 4, S5, and S6).** The survey scans (Figures **4c and 4d)** verified the presence of significant components: Nb, C, O, and F of Nb_2CT_z. Compared to the as-prepared Nb_2CT_z samples (**Figure 4c and 4d**). The deconvoluted spectra and quantified results of as-prepared and oxidized Nb_2CT_z samples are shown in **Figure 4, Figure S4, S5, Table S4, and Table S5.** The degree of oxidation was examined based on the XPS spectra: oxide peaks in the Nb 3d spectra, Nb_2C peak in the C 1s spectra, and the Nb_2O_5 component in the O 1s spectra. In the Nb 3d spectra (**Figures 4e and 4f**), we see the atomic fraction of oxides increase from 73.04% (in the as-prepared Nb_2CT_z) to 95.86% after storage for 300 hours. The increase in the oxide content shows the

poor oxidation stability of Nb_2CT_z. Similarly, the oxidation behavior are correlated with decreases in the Nb_2CT_z peak in the C 1s spectra: the MXene component (C-Nb-T_z) content decreased from 3.93% to 1.59% (**Figure S4a and S5a**). Finally, the change in the Nb_2O_5 peak in the O 1s spectra (**Figure S4b and S5b**) shows an increase in Nb_2O_5 content from 36.16% to 60.10% for the aged Nb_2CT_z samples. The increase in Nb_2O_5 at % in the O 1s spectra further reveals the poor oxidation stability of Nb_2CT_z.

Conclusions

In conclusion, molten salt etching of Nb_2CT_z is a promising method to manufacture non-Ti-based MXene. This approach provides a less hazardous way to make Nb_2CT_z nanosheet dispersions. The SEM, EDS, DLS, XRD XPS, and AFM confirm the formation of Nb_2CT_z. The Nb_2CT_z synthesis by molten salt etching can be scaled up for industrial production due to its less hazardous (non-HF) route. The data show that molten salt etched Nb_2CT_z is more stable against oxidation than acid etched Nb_2CT_z; we hypothesize that this is due to differences in their terminal groups.

Conflict of interest

There are no conflicts to declare.

Acknowledgments

Funding for the study was provided by supported by the US National Science Foundation (CMMI-1760859). We want to acknowledge the use of the TAMU Materials Characterization Facility and Microscopy & Imaging Center. We also acknowledge Dr. Mustafa Akbulut for the use of his group's ZetaSizer instrument. We would like to acknowledge Ava Crowley of TAMU for her help in Figure 1.

Notes and references

(1) Naguib, M.; Kurtoglu, M.; Presser, V.; Lu, J.; Niu, J.; Heon, M.; Hultman, L.; Gogotsi, Y.; Barsoum, M. W. Two-dimensional nanocrystals produced by exfoliation of Ti3AlC2. *Advanced materials* **2011**, *23*, 4248-4253.

(2) Naguib, M.; Mashtalir, O.; Carle, J.; Presser, V.; Lu, J.; Hultman, L.; Gogotsi, Y.; Barsoum, M. W. Two-dimensional transition metal carbides. *ACS nano* **2012**, *6*, 1322-1331.

(3) Naguib, M.; Mochalin, V. N.; Barsoum, M. W.; Gogotsi, Y. 25th anniversary article: MXenes: a new family of two-dimensional materials. *Advanced materials* **2014**, *26*, 992-1005.

(4) Sarang, K.; Zhao, X.; Holta, D.; Cao, H.; Arole, K.; Flouda, P.; Oh, E.-S.; Radovic, M.; Green, M. J.; Lutkenhaus, J. L. Carbon Additive-Free Crumpled Ti3C2T X MXene-Encapsulated Silicon Nanoparticle Anodes for Lithium-Ion Batteries. *ACS Applied Energy Materials* **2021**, *4*, 10762-10773.

(5) Seh, Z. W.; Fredrickson, K. D.; Anasori, B.; Kibsgaard, J.; Strickler, A. L.; Lukatskaya, M. R.; Gogotsi, Y.; Jaramillo, T. F.; Vojvodic, A. Two-dimensional molybdenum carbide (MXene) as an efficient electrocatalyst for hydrogen evolution. *ACS Energy Letters* **2016**, *1*, 589-594.

(6) Cao, H.; Escamilla, M.; Arole, K. D.; Holta, D.; Lutkenhaus, J. L.; Radovic, M.; Green, M. J.; Pentzer, E. B. Flocculation of MXenes and Their Use as 2D Particle Surfactants for Capsule Formation. *Langmuir* **2021**, *37*, 2649-2657.

(7) Kim, S. J.; Koh, H.-J.; Ren, C. E.; Kwon, O.; Maleski, K.; Cho, S.-Y.; Anasori, B.; Kim, C.-K.; Choi, Y.-K.; Kim, J. Metallic Ti3C2T x MXene gas sensors with ultrahigh signal-to-noise ratio. *ACS nano* **2018**, *12*, 986-993.

(8) Anasori, B.; Lukatskaya, M. R.; Gogotsi, Y. 2D metal carbides and nitrides (MXenes) for energy storage. *Nature Reviews Materials* **2017**, *2*, 1-17.

(9) Habib, T.; Patil, N.; Zhao, X.; Prehn, E.; Anas, M.; Lutkenhaus, J. L.; Radovic, M.; Green, M. J. Heating of Ti 3 C 2 T x MXene/polymer composites in response to Radio Frequency fields. *Scientific reports* **2019**, *9*, 1-7.

(10) Saha, S.; Arole, K.; Radovic, M.; Lutkenhaus, J.; Green, M. One-step hydrothermal synthesis of porous Ti3C2Tz MXene/rGO gels for supercapacitor applications. *Nanoscale* **2021**.

(11) Feng, A.; Yu, Y.; Jiang, F.; Wang, Y.; Mi, L.; Yu, Y.; Song, L. Fabrication and thermal stability of NH4HF2-etched Ti3C2 MXene. *Ceramics International* **2017**, *43*, 6322-6328.

(12) Lakhe, P.; Prehn, E. M.; Habib, T.; Lutkenhaus, J. L.; Radovic, M.; Mannan, M. S.; Green, M. J. Process Safety Analysis for Ti3C2T x MXene Synthesis and Processing. *Industrial & Engineering Chemistry Research* **2019**, *58*, 1570-1579.

(13) Wang, C.; Shou, H.; Chen, S.; Wei, S.; Lin, Y.; Zhang, P.; Liu, Z.; Zhu, K.; Guo, X.; Wu, X. HCl-Based Hydrothermal Etching Strategy toward Fluoride-Free MXenes. *Advanced Materials* **2021**, 2101015.

(14) Peng, C.; Wei, P.; Chen, X.; Zhang, Y.; Zhu, F.; Cao, Y.; Wang, H.; Yu, H.; Peng, F. A hydrothermal etching route to synthesis of 2D MXene (Ti3C2, Nb2C): Enhanced exfoliation and improved adsorption performance. *Ceramics International* **2018**, *44*, 18886-18893.

(15) Yin, T.; Li, Y.; Wang, R.; Al-Hartomy, O. A.; Al-Ghamdi, A.; Wageh, S.; Luo, X.; Tang, X.; Zhang, H. Synthesis of Ti3C2Fx MXene with controllable fluorination by electrochemical etching for lithium-ion batteries applications. *Ceramics International* **2021**, *47*, 28642-28649.

(16) Arole, K.; Blivin, J. W.; Saha, S.; Holta, D. E.; Zhao, X.; Sarmah, A.; Cao, H.; Radovic, M.; Lutkenhaus, J. L.; Green, M. J. Water-dispersible Ti3C2Tz MXene nanosheets by molten salt etching. *Iscience* **2021**, *24*, 103403.

(17) Urbankowski, P.; Anasori, B.; Makaryan, T.; Er, D.; Kota, S.; Walsh, P. L.; Zhao, M.; Shenoy, V. B.; Barsoum, M. W.; Gogotsi, Y. Synthesis of two-dimensional titanium nitride Ti 4 N 3 (MXene). *Nanoscale* **2016**, *8*, 11385-11391.

(18) Li, M.; Lu, J.; Luo, K.; Li, Y.; Chang, K.; Chen, K.; Zhou, J.; Rosen, J.; Hultman, L.; Eklund, P. Element replacement approach by reaction with Lewis acidic molten salts to synthesize nanolaminated MAX phases and MXenes. *Journal of the American Chemical Society* **2019**, *141*, 4730-4737.

(19) Li, Y.; Shao, H.; Lin, Z.; Lu, J.; Liu, L.; Duployer, B.; Persson, P. O.; Eklund, P.; Hultman, L.; Li, M. A general Lewis acidic etching route for preparing MXenes with enhanced electrochemical performance in non-aqueous electrolyte. *Nature Materials* **2020**, 1-6.

(20) Kamysbayev, V.; Filatov, A. S.; Hu, H.; Rui, X.; Lagunas, F.; Wang, D.; Klie, R. F.; Talapin, D. V. Covalent surface modifications and superconductivity of two-dimensional metal carbide MXenes. *Science* **2020**, *369*, 979-983.

(21) Azadmanjiri, J.; Reddy, T. N.; Khezri, B.; Děkanovský, L.; Parameswaran, A. K.; Pal, B.; Ashtiani, S.; Wei, S.; Sofer, Z. Prospective Advances in MXene Inks: Screen Printable Sediments for Flexible Micro-Supercapacitor Applications. *Journal of Materials Chemistry A* **2022**.

(22) Echols, I. J.; Holta, D. E.; Kotasthane, V. S.; Tan, Z.; Radovic, M.; Lutkenhaus, J. L.; Green, M. J. Oxidative Stability of Nb n+ 1C n T z MXenes. *The Journal of Physical Chemistry C*.

(23) Tezel, G. B.; Arole, K.; Holta, D. E.; Radovic, M.; Green, M. J. Interparticle interactions and rheological signatures of Ti3C2Tz MXene dispersions. *Journal of Colloid and Interface Science* **2022**, *605*, 120-128.

(24) Su, T.; Peng, R.; Hood, Z. D.; Naguib, M.; Ivanov, I. N.; Keum, J. K.; Qin, Z.; Guo, Z.; Wu, Z. One-step synthesis of Nb2O5/C/Nb2C (MXene) composites and their use as photocatalysts for hydrogen evolution. *ChemSusChem* **2018**, *11*, 688-699.

(25) Zhang, C.; Beidaghi, M.; Naguib, M.; Lukatskaya, M. R.; Zhao, M.-Q.; Dyatkin, B.; Cook, K. M.; Kim, S. J.; Eng, B.; Xiao, X. Synthesis and charge storage properties of hierarchical niobium pentoxide/carbon/niobium carbide (MXene) hybrid materials. *Chemistry of Materials* **2016**, *28*, 3937-3943.

(26) Song, S.; Liu, J.; Zhou, C.; Jia, Q.; Luo, H.; Deng, L.; Wang, X. Nb2O5/Nb2CTx composites with different morphologies through oxidation of Nb2CTx MXene for high-performance microwave absorption. *Journal of Alloys and Compounds* **2020**, *843*, 155713.

(27) Sarycheva, A.; Gogotsi, Y. Raman spectroscopy analysis of the structure and surface chemistry of Ti3C2T x MXene. *Chemistry of Materials* **2020**, *32*, 3480-3488.

(28) Huang, S.; Mochalin, V. N. Understanding chemistry of two-dimensional transition metal carbides and carbonitrides (MXenes) with gas analysis. *ACS nano* **2020**, *14*, 10251-10257.

(29) Gao, L.; Chen, H.; Zhang, F.; Mei, S.; Zhang, Y.; Bao, W.; Ma, C.; Yin, P.; Guo, J.; Jiang, X. Ultrafast relaxation dynamics and nonlinear response of few-layer niobium carbide MXene. *Small Methods* **2020**, *4*, 2000250.

(30) Iqbal, A.; Hong, J.; Ko, T. Y.; Koo, C. M. Improving oxidation stability of 2D MXenes: synthesis, storage media, and conditions. *Nano Convergence* **2021**, *8*, 1-22.

This journal is © The Royal Society of Chemistry 20xx